Received: 3 May 2021 | Revised: 30 September 2021 | Accepted: 1 October 2021

DOI: 10.1002/app.51784

ARTICLE

Applied Polymer SCIENCE WILEY

Synthesis and properties of neat, hybrid, and copolymeric polyamide 12 microparticles and composites on their basis

Nadya Vasileva Dencheva | **Joana Filipa Barros Braz** | **Zlatan Zlatev Denchev**

IPC-Institute for Polymers and Composites, University of Minho, Campus of Azurem, Guimarães, Portugal

Correspondence
Zlatan Zlatev Denchev, IPC-Institute for Polymers and Composites, University of Minho, Campus of Azurém, 4800-Guimarães, Portugal.
Email: denchev@dep.uminho.pt

Funding information
Fundação para a Ciência e a Tecnologia, Grant/Award Numbers: UID/CTM/50025/2019, CTTI-51/18-IPC, UI/BD/150854/2021; Universitat Autònoma de Barcelona, Grant/Award Number: ALBA synchrotron project ID 2018/022726

Abstract

Neat and hybrid polyamide 12 (PA12) based powders are important raw materials for additive manufacturing. This study describes a facile method for the synthesis of pure, hybrid and copolymeric microparticulate materials based on one-pot activated anionic ring-opening polymerization (AAROP) of laurolactam in solution. The results reveal the possibility to obtain in good yields, for reaction times of 2 h and temperatures of up to 110°C neat and hybrid PA12 microparticles (MP) carrying metal or carbon fillers. Copolymeric PA12/PA6 MP can also be successfully prepared. All MP materials are analyzed by spectral, microscopy, thermal, and synchrotron X-ray scattering methods in order to clarify their morphology, chemical and crystalline structure, melting and degradation behavior. The melting temperature of the PA12 MP is lower than of the commercial PA12, the presence of metal particles or copolymerization with PA6 additionally decrease it well below 170°C. The composites prepared by compression molding of PA12 MP display elastic modulus of up to 1.49 GPa, the stresses at yield and break reaching 50 and 69 MPa, respectively. It is concluded that the neat, hybrid, and copolymeric pulverulent materials obtained via microencapsulation by AAROP in solution may be useful in additive manufacturing processing.

KEYWORDS

copolymers, polyamides, ring-opening polymerization, synthesis and processing techniques, thermal properties

1 | INTRODUCTION

Polyamide 12 (PA12) possesses a valuable set of properties representing a combination of polyolefins' low moisture absorption and reduced density accompanied by a chemical resistance and mechanical properties being similar or even better than those of the typical polyamides. For example, PA12 shows impact strength and Young modulus superior to those of polyamide 6 (PA6) and higher elongation at break than PA6 and PA66.[1,2] This makes neat PA12 and the composite materials on its basis useful in a wide range of applications, especially in automotive and electrical industries, as well as in precision molding, sports and leisure goods.[3] Most of the commercial PA12 is produced by hydrolytic polycondensation at 260–300°C, and only a small market volume is prepared by activated anionic ring-opening polymerization (AAROP) of laurolactam in bulk.[1] There exist steady academic and industrial interest to PA6-PA12 copolymers obtained by both techniques.[4–6]

The advent of additive manufacturing technology gave a powerful impetus to a number of layer-by-layer production techniques, one of the most promising of them being the selective laser sintering (SLS). It uses

pulverulent materials transforming them into solid three-dimensional parts by means of laser beam.[7] The correct choice of powder material with suitable particle size, shape, rheology, and crystallization behavior is fundamental for the successful sintering to final articles with optimized mechanical properties.[8,9]

Among polymer raw materials for SLS, the polyamide powders are currently the most widely used especially PA12 that makes up more than 95% of the current market owing to its wide processing window and relatively low melt viscosity.[10] The dissolution-precipitation[11,12] is the most popular method for preparing PA12 powders for SLS, in which porous microparticles (MP) are produced with nearly spherical, potato-like shape. A common disadvantage of this method is the difficulty in finding suitable solvents and precipitants for polyamides. Melt emulsification is another approach for obtaining PA12 or other polymer powders with a near-spherical shape.[13] The particles prepared usually have a rather broad size distribution that makes necessary additional sieving into 10–150 μm range considered ideal for SLS.[14] Cryogenically milling of PA12 pellets also produces powders with very broad particle size distribution, also requiring sieving. Moreover, this method yields particles with irregular form that can result in porous and mechanically weak SLS parts.[8,9,15] Very recently, a new method based on physical phenomena that is, the Plateau-Rayleigh instability of molten fibers was used to prepare PA12 powders.[16] There, PA12 fibers are first prepared by melt spinning, cropped to oriented pellets and dispersed in molten polyethylene oxide (PEO), followed by heat-treatment at temperatures higher than the melting point of PA12. After cooling, the water-soluble PEO phase is removed by washing away with deionized water and the solid residue is dried to obtain the PA12 powders containing nearly spherical PA12 MP proved to be especially useful for SLS. This procedure is rather complex, could be costly for scaling and requires two high-temperature treatments that may change unfavorably the crystalline structure and the melting properties of PA12.

PA12 MP can be prepared not only by physical methods but also by AAROP of lactams in an appropriate solvent. Thus, Senff and Gaboriau from Arkema Inc.[17] disclosed the preparation of polyamide (including PA12) MP by AAROP of the respective lactam in a hydrocarbon solvent with a boiling point between 120–170°C. As anionic initiator NaH was used, and as co-initiator – isocyanate compounds that react with the lactam monomer to form in-situ the imide activator compound. By this method PA12 and PA6 homopolymer MP were synthesized, as well as copolymer PA12-6 ones containing small amount of silica as nucleating agent and low molecular weight substituted amides as stabilizers. More recently, Denchev and Dencheva[18] suggested the synthesis of polyamide MP (including such of PA12) by AAROP in solution employing a catalytic system composed by a sterically hindered anionic initiator and a bifunctional imide activator, both of them being commercially available. This process permitted the preparation of polyamide MP based on PA6, carrying elevated amounts of fillers, i.e., metal-, ceramic-, carbon allotrope or mixed payloads, as well as other polymer particles. Further investigations revealed that these hybrid MP can be used directly as supports for enzymes in biosensors or biocatalysts[19,20] or they can be transformed by melt processing into PA6-based hybrids or laminate composites.[21,22] The procedure of ref. [18] was also used for the preparation of PA4 hybrid MP with a potential application as biodegradable enzyme supports[23] or for selective recognition of biomolecules.[24]

This work is the first report on the structure and morphology of neat and hybrid PA12 MP prepared by AAROP of laurolactam (LL) in solution, carrying certain amounts of metal or carbon allotrope payloads. Copolymeric PA12-6 MP were produced analogously using a mixture of LL and ε-caprolactam (CL). These MP were transformed into plates by compression molding. The morphology and structure of all MP and molded plates were studied by microscopic, spectral, thermal, mechanical, and X-ray scattering techniques. Conclusions were made about the applicability of the neat, hybrid, and copolymeric PA12-based MP in SLS or for the preparation of bulk hybrid composite materials.

2 | EXPERIMENTAL

2.1 | Materials

The CL monomer with reduced moisture content for AAROP (AP-Nylon® caprolactam) was delivered from Brüggemann Chemical, Germany. The LL monomer (purity >99%) was purchased from Merck, Portugal. Before use, both were dried under vacuum at 60°C. As activator of the AAROP of ECL the commercial product Brüggolen C20 from Brüggemann Chemical (Germany) was employed containing, according to the manufacturer, 80 wt% of aliphatic diisocyanate blocked in CL. The polymerization initiator sodium dicaprolactamato-bis-(2-methoxyethoxo)-aluminate (Dilactamate, DL), which is also a commercial product was supplied by Katchem (Czech Republic) and used without further treatment. The acetylene carbon black (CB) is a product of S.E.A. Tudor, Spain with average particle sizes in the 10–50 nm range. Aluminum powder (99.9% Al, particle size <30 μm) were supplied by Merck, Portugal. Soft, non-insulated

iron particles (Fe content >99.8%), with average diameters of 3–5 μm were kindly donated by the manufacturer BASF, Ludwigshafen, Germany. Methanol, toluene, xylene, and other solvents are of 'puriss' grade purchased from Merck, Portugal and used as received.

2.2 | Sample preparation

The AAROP was carried out in a 250 ml glass flask fitted with thermometer, magnetic stirrer, a Dean-Stark attachment for azeotropic distillation with a reflux condenser and inlet for nitrogen. In a typical synthesis, 0.2 mol of LL, (or, in the case of copolymer synthesis, a mixture of 0.1 mol CL and 0,1 mol LL) were admixed to 2 wt% of the respective filler (Al, Fe, or CB particles) and then blended with 80–100 ml of 1:1 toluene/xylene mixture. The reaction mixture was stirred under nitrogen atmosphere refluxing for 10–15 min. Subsequently, 3 mol% of DL and 1.5 mol% of C20 were added at once (all weight percentages are in respect to the lactam monomer[s]). The reaction time was always 2 h measured from the point of catalytic system addition. The temperature was maintained in the 110–120°C range, at a constant stirring of ca. 800 rpm. The PA12 MP without or with payload formed as white or gray powders, depending on the payload employed. The MP were separated from the reaction mixture by hot vacuum filtration, washed several times with methanol, Soxhlet extracted with methanol for 4 h, and then dried for 30 min at 80°C/50 mbar in a vacuum oven.

Compression molding of MP to plates was performed in a 25 ton Moore hydraulic hot press (UK), using a rectangular mold with dimensions 85 × 75 × 1 mm, pressing for 5–7 min at 200–220°C, applying a pressure of 10 MPa. Control samples of hydrolytic PA12 (HPA12) were produced analogously by compression molding of granules of Grilamid L of EMS-Grivory, Switzerland.

2.3 | Characterization

Bright field optical microscopy measurements of MP sizes, roundness and their distributions were performed in an BH-2 microscope (Olympus Corp., Japan) equipped with a DFC200 (Leica Microsystems, Manheim, Germany) digital camera using the Leica Application Suite 4.4 software for image processing. The scanning electron microscopy (SEM) studies were performed in a NanoSEM-200 apparatus of FEI Nova (Hillsboro, USA) using mixed secondary electron/back-scattered electron in-lens detection. The MP samples were observed after sputter-coating with Au/Pd alloy in a 208 HR equipment of Cressington Scientific Instruments (Watford, UK) with high-resolution thickness control.

The average viscometric molecular weights M_v of the neat PA12 and the PA12-6 copolymer were determined by intrinsic viscosity measurements in 97% sulfuric acid at a concentration of 0.2 g/dl with a suspended level Ubbelohde viscometer thermostatted at 25°C. The Mark-Houwink equation for PA12 was used with $K = 5.24 \cdot 10^{-4}$ and $\alpha = 0.73$.[1] Flow times were recorded as an average of five runs.

The infrared spectra of selected MP samples were obtained in a JASCO FTIR-4600 (FTIR stands for fourier transform infrared spectroscopy) apparatus (Tokyo, Japan) at room temperature, with a resolution of 4 cm^{-1} accumulating up to 64 spectra for optimum signal-to-noise ratio. The MP powders were studied with either ATR attachment or in KBr pellets, in the latter case in transmission mode.

The differential scanning calorimetry (DSC) measurements were carried out in a 200 F3 equipment of Netzsch (Selb, Germany) at a heating rate of 10°C/min under nitrogen purge. The typical sample weights were in the 10–15 mg range. The effective inorganic load in MP was established by means of thermogravimetric analysis (TGA) in a Q500 gravimetric balance (TA Instruments, New Castle, USA) heating the samples to 600°C at 10°C/min in N_2 atmosphere. The real load R_L of filler in MP was calculated according to Equation (1):

$$R_L = R_i - R_{PA12} \times 100, [\%] \quad (1)$$

where R_{PA12} is the carbonized residue at 600 °C of empty MP and Ri – that of the respective loaded MP measured by TGA.

The tensile tests were performed in an Instron 4505 testing machine (Norwood, USA) at 23 ± 2°C with a standard load cell of 50 kN at a constant crosshead speed of 50 mm/min. From the different composite plates prepared by compression molding of MP, standard specimens were cut out according to DIN 53504-S3. At least five specimens of each molded sample were studied to calculate the average values and their standard deviation. The engineering stress σ was determined as the ratio of the tensile force to the initial cross-section of the sample. The engineering strain ε was determined as the ratio of the sample gauge length at any time during drawing to that before drawing. The Young's modulus E values were calculated from the initial slope of the stress–strain curves (up to 1% strain). In all cases conditioned samples stored for ca. 30 days at 23°C and 65% relative humidity were tested.

Synchrotron wide (WAXS) and small-angle X-ray scattering (SAXS) measurements were performed in the

NCD-SWEET beamline of the ALBA synchrotron facility in Barcelona, Spain.[25] Two-dimensional detectors were used, namely LH255-HS (Rayonix, USA) and Pilatus 1 M (Dectris, Switzerland) for registering the WAXS and SAXS patterns, respectively. The sample-to-detector distance was set to 150.3 mm for WAXS and 2696.5 mm for SAXS measurements, the λ of the incident beam being 0.1 nm and the beam size 0.35 × 0.38 mm (h × v). The 2D data from the two detectors were reduced to 1D data using pyFAI software.[26] For further processing of the WAXS and SAXS patterns the commercial package Peakfit 4.12 by SeaSolve was implemented.

3 | RESULTS AND DISCUSSION

3.1 | Synthesis of the PA12-based MP

The chemical structures of the LL, C20 activator, DL anionic initiator and the theoretical composition of the forming PA12 macromolecule are presented in Figure 1.

As well-known from our previous studies with CL,[27–29] the AAROP involves a reaction of the lactam anion initiator DL with the imide links –C(O)-N-C(O) of the activator C20, followed by fast proton exchange of the adduct with a monomer molecule and restauration of the lactamate anion. The result of this reaction sequence is the propagation of the PA12 chain. Having in mind that the C20 compound contains two imide links, chain propagation in both directions should be expected, which explains the necessity of a 2:1 molar ratio of the DL:C20.

Since the C20 active imide compound belongs to the group of the fast activators, to obtain MP and not fused agglomerates or chunks of bulk polymer, the relatively slow initiator DL was selected. Due to the coordination of the lactamate anion with the aluminum ligand (Figure 1), a decreased nucleophilicity is achieved in DL combined with effective delocalization of the negative charge. In fact, the present study proves that using the DL/C20 catalytic system allows the successful synthesis of homopolymeric PA12 and copolymeric PA12-6 MP, whereby these MP can also contain particulate inorganic payloads that do not inactivate the catalytic system. The sample designations, polymerization yields along with some other characteristics of all MP samples are summarized in Table 1.

As seen from Table 1, the average viscosity molecular weights $\overline{M_v}$ of the filler-free PA12 MP and the PA12-6 copolymeric MP (1:1 by mol) are 33.8 and 28.9 kD, respectively. This is comparable to the average values of commercial hydrolytic PA12 [1]. The $\overline{M_v}$ of the metal- and CB-loaded PA12 MP could not be determined correctly due to the formation of fine, insoluble in H_2SO_4 and possibly inorganic colored precipitates, most probably representing metal and CB sulfates. As the payloads did not seem to influence the activity of the catalytic system and the well-established mechanism of AAROP, the $\overline{M_v}$ of the hybrid PA12 MP is expected to be around 30.0 kD as well.

The formation of PA6 MP in the process of AAROP in a hydrocarbon solvent was explained by Vasiliu-Oprea and Dan.[29] Initially, the growing polyamide chains fold and form viscous droplets representing coiled oligomer molecules. These droplets, upon additional chain propagation, coalescence and crystallization, produce the final semicrystalline MP. It can be hypothesized that the

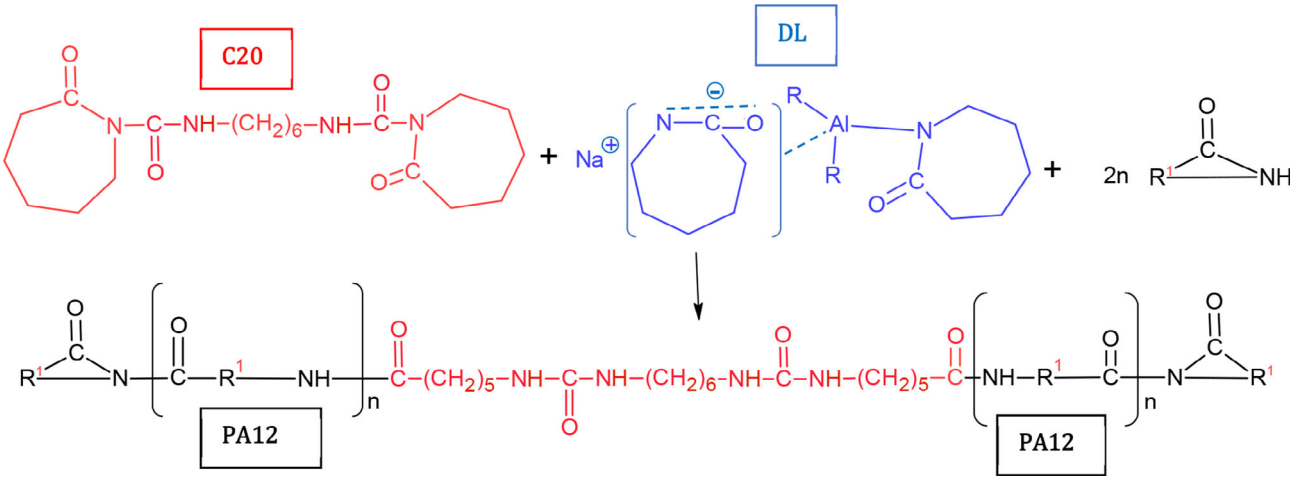

FIGURE 1 Chemical reactions occurring during AAROP of laurolactam ($R^1 = [CH_2]_{11}$) to PA12 MPs. In the case of PA12-6 copolymer, $R^1 = (CH_2)_{11}$ and $(CH_2)_5$ (1:1 mol ratio). The active substance of the AAROP activator is designated as C20; the chemical structure of the AAROP initiator dicaprolactamato-bis-(2-methoxyethoxo)-aluminate (DL) is presented wherein $R = OCH_2CH_2OCH_3$ [Color figure can be viewed at wileyonlinelibrary.com]

TABLE 1 Designation and some characteristics of the PA12 MP samples

Sample microparticles	MP yield, (%)[a]	Real filler content, R_L, (%)[b]	M_v kD	d_{max}, (μm)	d_{max}/d_{min}
PA12	25.3	—	33.8	15–30	1.2–1.6
PA12-Fe	58.5	6.0	—[c]	15–30	1.2–1.6
PA12-CB	73.0	3.2	—[c]	15–35	1.2–1.5
PA12-Al	53.0	3.7	—[c]	15–35	1.2–1.5
PA12-6 1:1	77.1	0.0	28.9	10–25	1.2–1.6

[a]In relation to the lactam monomer, after 2 h reaction time.
[b]Determined by TGA according to Equation 1.
[c]Viscosity measurements cannot be performed correctly. For details see the text.

formation of PA12-based homo- and copolymeric neat MP will follow a similar pathway. Any metal or carbon load particle will be entrapped into the viscous PA12 coiled structures and will possibly nucleate their crystallization thus forming hybrid PA12 particles. Notably, the yield of neat PA12 powder is the lowest and the AAROP in this case tends to produce big lumps instead of the desired MP. This lumping effect is weak in the loaded PA12 samples and completely missing in the PA12-6 MP. Most probably, the reason is the easy heteronucleation in the forming PA12 hybrid MP caused by the filler particles. In the PA12-6 MP sample, it is the PA6 blocks that crystallize easier and nucleate the crystallization of the PA12 ones. After their crystallization, the MP precipitate and exit the AAROP chain growth process. This will be more difficult in the neat PA12 sample where homo nucleation is only possible since no surfactant was used in any of the AAROP syntheses.

PA12 yields (in respect to the monomer LL) in the range of 25% for neat MP and 54%–73% for the PA12 hybrid MP and PA12-6 copolymeric MP were obtained (Table 1). Notably, the amount of the solid loads introduced in AAROP was always 2 wt % in respect to the LL monomer. In the final hybrid MP samples, the real payload percentage determined by TGA is 3–6 wt% mostly due to the fact that a significant fraction of the monomer is not transformed into polyamide while at the same time all payload particles are entrapped into the forming polymer MP due to the insolubility of Al, Fe or CB in the AAROP solvent.

3.2 | Morphological studies by SEM and energy dispersive X-Ray analysis

As seen from Table 1, columns 5 and 6 (data obtained from optical microscopy), PA12 neat and hybrid MP display similar sizes, most particles being within the 15–35 μm range, which is considered excellent for SLS. The copolymeric PA12-6 MP sample presents smaller particles. In all MP samples, the form of the particles is relatively irregular, the relation between the maximum and minimum sizes d_{max}/d_{min} being in the range of 1.2–1.6.

More details on the MP morphology can be found by SEM. Figure 2 provides visual information on the size, shape and surface topography of PA12 MP obtained by AAROP. From the micrographs of the PA12 MP sample (Figure 2, 1a, c) it can be seen that the selected particle is a bit larger than 20 μm, with irregular form. The surface topology at the largest magnification seems to be a combination of solid and porous segments. The PA12-CB sample (images 2a–c) display larger aggregated entities with sizes close to 50–60 μm, whose surface is predominantly porous. In the Al-containing PA12 MP (3a-3c) the typical particles' size is between 20–30 μm with mixed porous-solid topography.

The copolymer PA12-6 sample (Figure 2, 4a–c) displayed size of the particles of up to 20 μm with a surface being rather different than that of all other PA12-based samples. In Figure 2, image 4c one can observe some pores of submicron size, as well as indications of polymer brush morphology composed of multiple tethered bottlebrush polymer chains. This specific morphology develops only in the copolymeric sample.

The EDX analysis of the PA12-Al sample (Figure 3 a, b) proves that the metal payload is not found on the MP surface (no Al signal in site Z2), but in the surface defects, as the K_a of Al is only seen if the electron beam is directed into the superficial cracks in MP (site Z1). Sample PA12-Fe (not shown in Figures 2 and 3) has a similar morphology with the metal particles being in the interior of the MP. The MP can contain one or more metal particles, depending on their sizes (3–5 μm for Fe and < 30 μm for Al).

The PA12-CB sample micrograph in Figure 3c allows the distinction of the carbon particles as brighter submicron spherical inclusions with diameters of 100–120 nm, well dispersed upon the porous surface of the

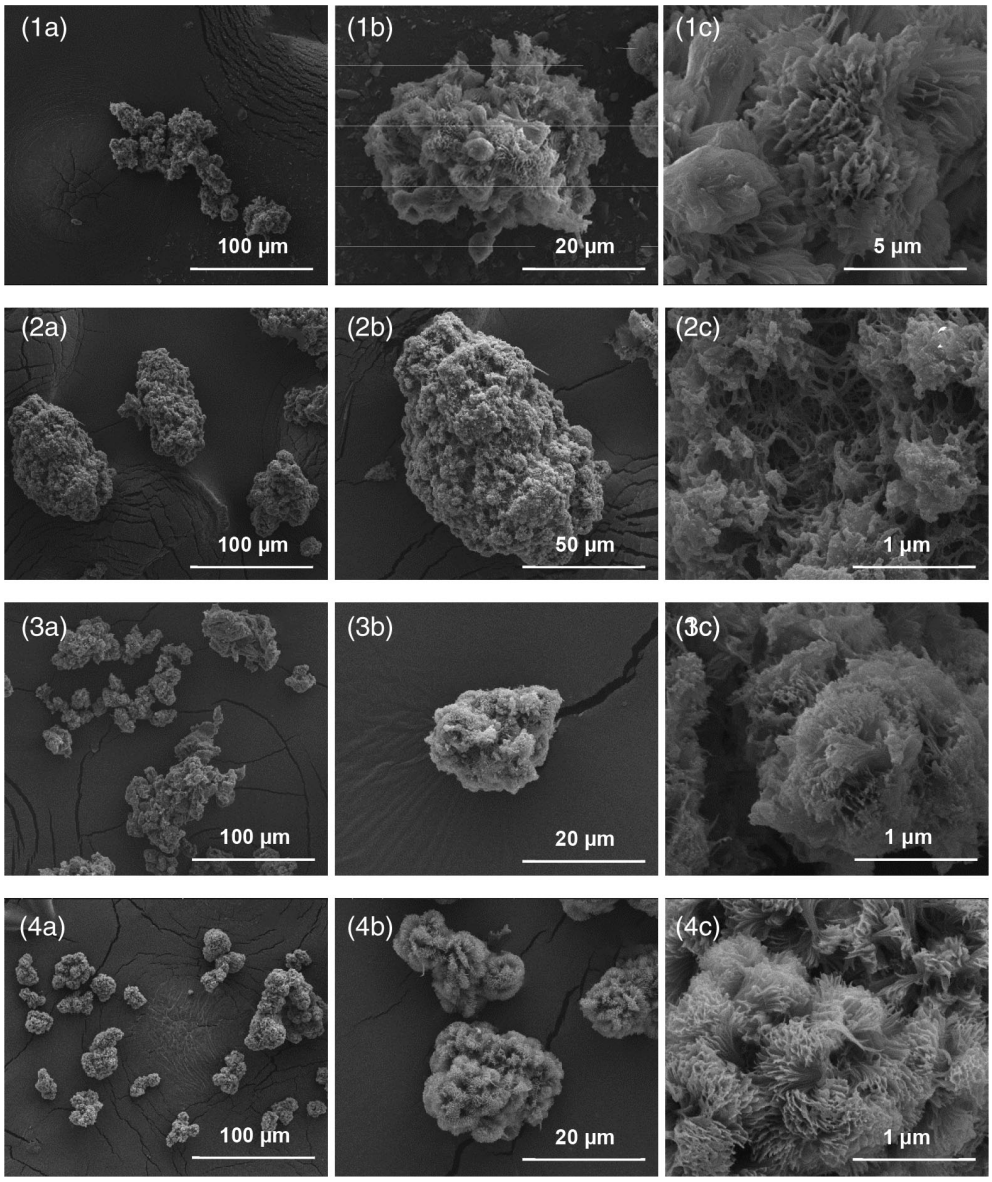

FIGURE 2 Selected scanning electron microscopy (SEM) micrographs of MP with different magnifications and loads: 1a -1c – PA12; 2a-2c – PA12-CB; 3a-3c – PA12-Al; 4a-4c – PA12-6

MP and, most probably, within the interior of the MP as well.

3.3 | Structural studies by FTIR

FTIR spectroscopy was used to study the chemical structure of the neat and hybrid PA12 MP. A special attention was given to the structure of the copolymeric PA12-6 MP. The full spectra of neat PA12 and PA12-6 MP are presented in Figure 4. For better understanding and comparison, the spectrum of PA6 MP prepared in the same way is also presented.

The three samples display quite similar spectra in the 4000–600 cm^{-1} being typical of PA6 and PA12.[30,31] Thus, the bands at 3298–3300 cm^{-1} are assigned to hydrogen-bonded stretching vibrations in secondary NH groups. The bands at 3081–3089 cm^{-1} should be attributed to the NH-stretching of the Amide II group. The two bands centered at 2920 and 2848 cm^{-1} are characteristic of the methylene groups' symmetric stretching vibrations. Their relative intensity corresponds to the number of the CH_2 groups in the repeat unit of PA6 and PA12. Also, the three spectra show well defined peaks for Amide I at 1635 cm^{-1} and Amide II at 1539 cm^{-1}. This is a clear indication for fixation of the trans-conformation of the NH-CO group, being typical for aliphatic amides and polyamides, thus excluding the presence of LL, CL or their cyclic oligomers in the final MP. The PA6 spectrum displays weak but detectable peak at 1710 cm^{-1} attributable to terminal carboxyl groups that result from partial opening of the terminal lactam cycles (Figure 1). In the PA12 and PA12-6 samples such peaks are not registered.

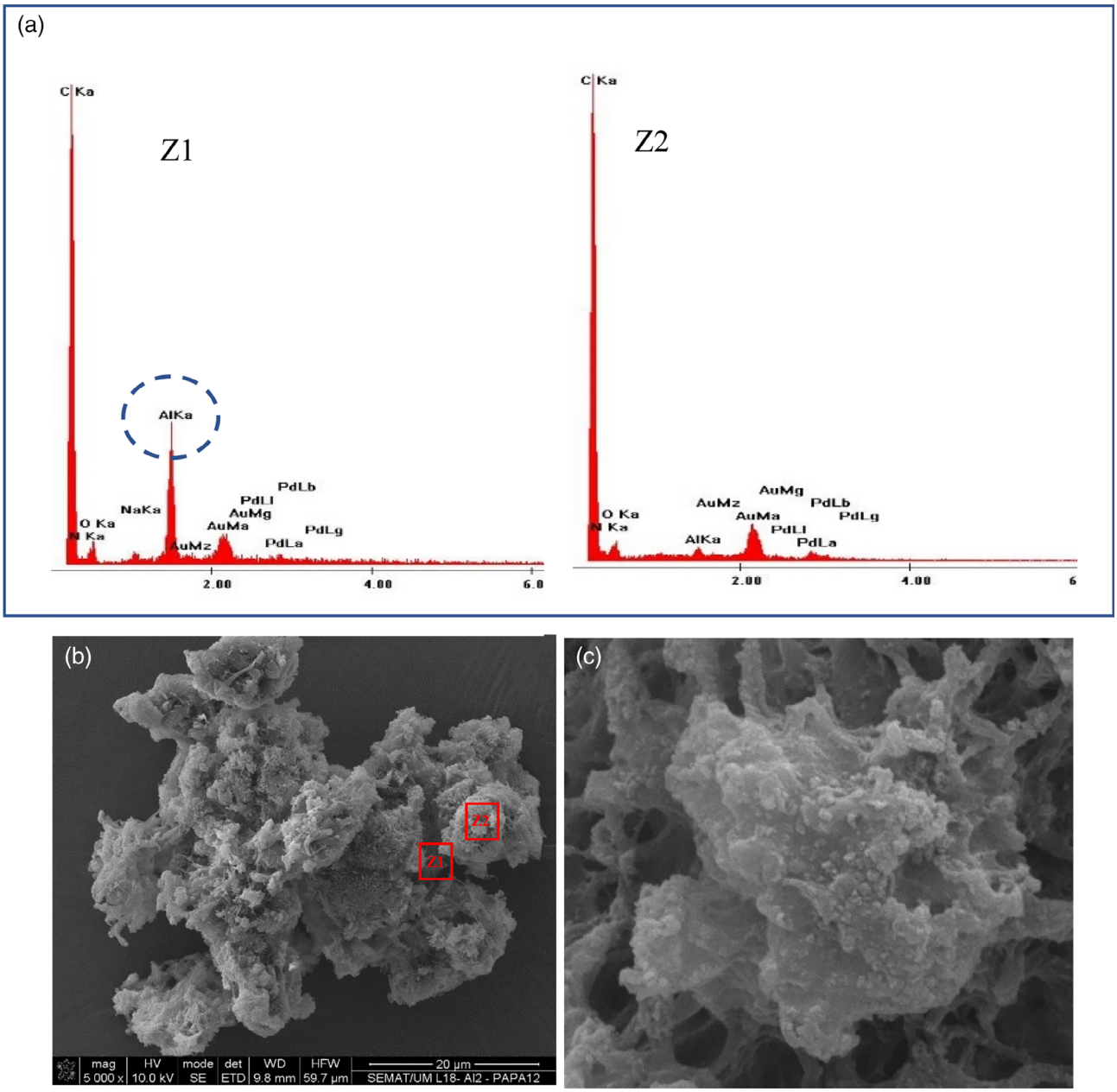

FIGURE 3 (a) and (b) energy dispersive X-Ray analysis (EDX) analysis of the PA12-Al sample in two different points – Z1 and Z2; (c) close-up of the PA12-CB [Color figure can be viewed at wileyonlinelibrary.com]

The hybrid PA12 samples with metal and carbon loads display spectra analogous to those in Figure 4 with the same groups of absorption bands appearing at similar wavenumbers. The only difference is that the respective peaks are somehow broader indicating higher heterogeneity of the samples.

The spectra in Figure 4 display some structural differences in the "finger print" area between 800–500 cm^{-1} that are worth analyzing. An extension of this spectral region is presented in Figure 5.

One of the bands in Figure 5 common for PA6, PA12 and the PA12-6 copolymer is centered at ca. 720 cm^{-1}. Based on previous detailed spectral studies on PA6 and PA12,[30,31] it can be assigned to the rocking vibrations of more than four consecutive methylene groups. As expected, the relative intensity of this band is higher in PA12 with 11 CH_2 groups in the repeat unit (curve 2) and in the PA12-6 copolymer (curve 3) than in PA6 MP (curve 1) with five CH_2 groups (Figure 1). The band at 685 cm^{-1} (more intense in PA6 and the PA12-6 samples compared to PA12) is assigned to the C═O group out-of-plane bending that is typical of the polyamide α-type polymorph. Apparently, PA6 and PA12-6 samples are richer in this polymorph than PA12. The well-expressed

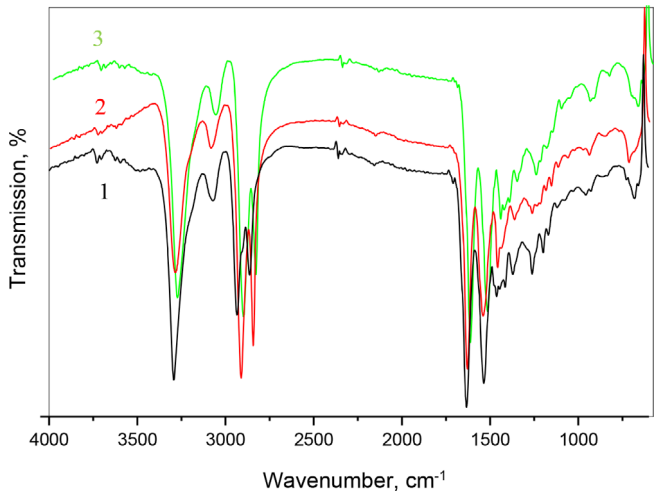

FIGURE 4 Full FTIR spectra of empty microparticles: 1 – PA6; 2 – PA12; 3 – PA12-6. Samples studied in ATR mode [Color figure can be viewed at wileyonlinelibrary.com]

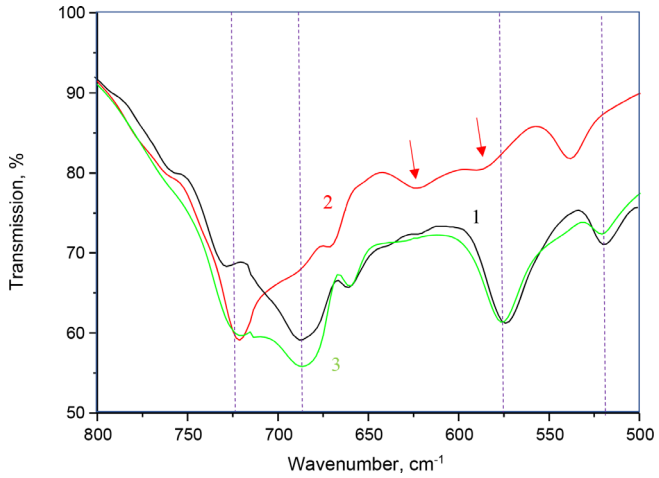

FIGURE 5 FTIR spectra of empty microparticles in the area of 800–500 cm^{-1} (KBr pellets studied in transmission mode): 1 – PA6; 2 – PA12; 3 – PA12-6 [Color figure can be viewed at wileyonlinelibrary.com]

peaks at 575 cm^{-1} that are common for PA6 and PA6-12 belong to the NH out-of-plane bending of the same α-polymorph. In PA12 this peak is shifted to 586 cm^{-1} (the right red arrow) and is with lesser intensity. The PA12 sample contains also a stronger peak at 623 cm^{-1} (left red arrow) related to the γ-PA12. Another band appearing at 521 cm^{-1} for PA6 and PA12-6 and 538 cm^{-1} for PA12 is attributable to the skeletal deformations of the α-crystalline phase. Unfortunately, rigorous quantification of the α- and γ-polymorphs based on the FTIR spectra was not possible. However, the FTIR data confirm indirectly the formation of high-molecular homo- and copolymeric MP, free of monomers and cyclic oligomers, with different α/γ polymorph content depending on the polyamide type and repeat unit composition.

3.4 | Thermal studies by DSC and TGA

The MP samples were subjected to DSC heating and cooling scans so as to study their melting and crystallization behavior. The five PA12 MP samples were compared to neat PA6 MP obtained in a similar AAROP synthetic process.[21] The DSC curves are presented in Figure 6 that shows the initial heating scan at 10°C/min, followed by a cooling cycle and a second heating scan at the same rate. Al data extracted from the thermograms are presented on Table 2. The DSC crystallinity index X_c^{DSC} was calculated as:

$$X_c^{DSC} = \frac{\Delta H_m^i}{V_f . \Delta H_m^0} \times 100, \% \quad (2)$$

wherein ΔH_m^i is the enthalpy of melting of the respective MP sample, and ΔH_m^0 stays for the enthalpy of melting of a 100% crystalline PA12 (209.2 J/g)[32] or PA6 (190 J/g).[22] In the case of the PA12-6 copolymer, to calculate the X_c^{DSC}, equal fractions $V_f = 0.5$ of both polyamides are considered.

All thermograms of the first heating scan (Figure 6a) display broad endotherms centered in the 65–75°C range, not appearing during the second heating scan (Table 2). These broad endotherms could be attributed to two possible causes: (i) Evaporation of solvents used in the synthesis or isolation of MP, or (ii) Release of internal tensions and readjustments of the porous structure (physical aging) of the MP. The later reason seems to be more probable since the more porous PA6 and PA12-6 microparticulate samples display more intense endotherms than the less porous PA12 MP.

Figure 6 and Table 2 prove that the presence of payload decreases the melting temperature T_m during the first heating scan. Thus, the empty PA12 MP melt at 174°C and those with Fe, CB or Al fillers – around 165–166°C (Figure 6a, curves 1–4). The fact that the payload of the PA12 MP can decrease the melting temperature of the matrix material with about 10°C is important for the application of these powders in SLS. As expected, the PA6 MP (curve 6) displayed T_m values of >200°C, as already shown in previous communications.[21] The degree of crystallinity X_c^{DSC} determined from the ΔH_m during the first heating scan vary between 36% and 39%, the difference between samples 1–4 being within the margin of

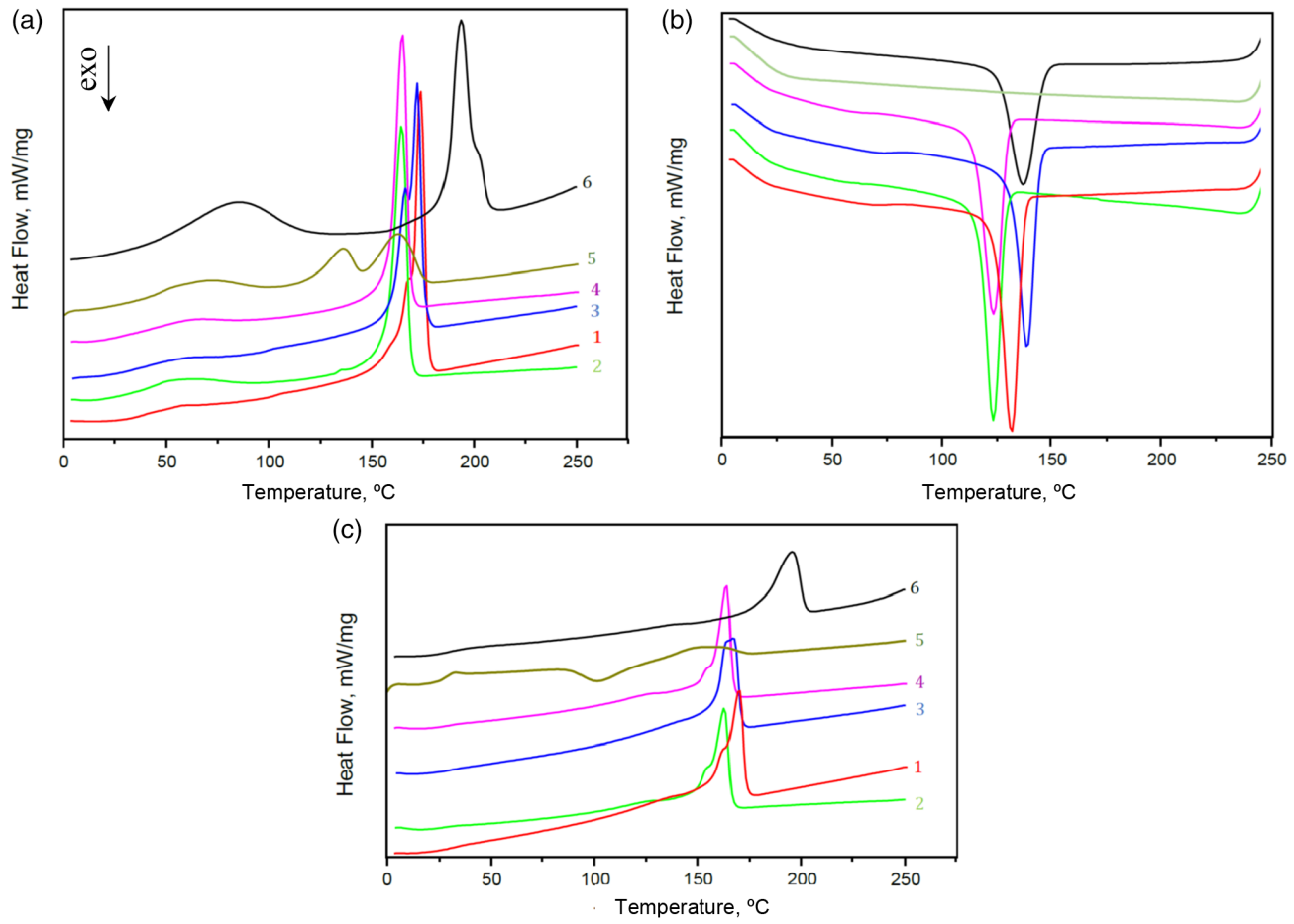

FIGURE 6 DSC traces of MP with different loads: a, First heating scan; b, Cooling scan; c, Second heating scan. 1 – PA12; 2 – PA12-Fe; 3 – PA12-CB; 4 – PA12-Al; 5 – PA12-6; 6 – PA6. The curves are shifted along the y-axis for better visibility [Color figure can be viewed at wileyonlinelibrary.com]

TABLE 2 Thermal data extracted from the DSC traces of MP samples in heating and cooling scans

Sample microparticles	T_g[a] (°C)	T_m[a] (°C)	T_c[a] (°C)	ΔH_m[a] (J/g)	ΔH_c[d] (J/g)	X_c^{DSC}, (%)[a]
PA12	42.3	173.8	131.9	80.9	−53.3	38.7
	30.1	169.9		50.0		23.9
PA12-Fe	42.0	164.8	123.7	76.5	−44.0	36.6
	28.1	162.8		44.9		21.5
PA12-CB	41.0	172.4[b] 166.0	138.8	79.6	−50.0	38.0
	23.7	167.1		47.1		22.5
PA12-Al	41.4	165.2	123.6	74.2	−49.5	35.7
	28.8	164.1		44.0		21.0
PA12-6	45–50	162.3 135.7	—	22.8 11.3	—	24.0 10.8
	28.5	156.3 101.0[c]		14.0 −8.6[c]		7.7

[a]Top row value registered in the first heating, bottom row value in the second heating scan.
[b]Dual melting peak.
[c]Crystallization peak obtained in the 1st heating scan.
[d]Values obtained in the cooling scan.

the experimental error. The copolymeric PA12-6 sample displays a quite distinct melting/crystallization behavior during the first scan. As seen from Figure 6a curve 5, typical dual melting is observed with $T_m^1 = 162°C$ ascribed to the PA6 blocks and $T_m^2 = 136°C$ ascribed to the PA12 blocks, both temperatures being with ca. 40°C lower than those of the neat PA6 and PA12 homopolymers. This is an indication that the PA12-6 MP is a block copolymer with crystallizable but relatively short blocks and not a mixture of homopolymers. The X_c^{DSC} indices of the PA6 and PA12 fractions calculated according to Equation 2 were 24% and 11%, respectively. A poorly resoled T_g was found in this sample in the 45–50°C range. The rest of the MP samples displayed T_g values of 41–42°C typical of conditioned PA12.

The DSC traces in cooling mode presented in Figure 4b displayed well-expressed crystallization peak temperatures T_c, whereby the value of the empty PA12 MP of ca. 132°C appeared between the T_c of the metal-loaded PA12-Al and PA12-Fe (123.7°C) and that of PA12-CB and neat PA6 MP – ca. 139°C. Notably, the PA12-6 copolymeric MP sample shows no crystallization at a cooling rate of 20°C/min.

Figure 6c displays the DSC traces of the second heating scan obtained after melting and recrystallization of MP. In Table 2 the respective thermal parameters are given as a second line to each sample designation. It can be seen a significant decrease of the T_g values during the second scan, in average with 15–18°C. This effect can be attributed to the lesser crystallinity of the recrystallized MP samples, which can be seen by comparing the X_c^{DSC} indices before and after MP recrystallization (Table 2, last column). The PA12-6 sample still produces some melting endotherm $\Delta H_m = 8.6$ J/g at 155°C, preceded by a crystallization peak with similar entropy of melting, that is, this crystalline phase was created during the second heating scan itself. Most probably transamidation reactions that occurred during the first scan led to formation of statistical copolymer. This assumption is supported by the fact that PA12-6 MP did not crystallize upon cooling. Small crystallization peak occurs only after reheating at temperatures above T_g, which in this case is very well expressed.

Summarizing, the DSC traces of PA12 neat, hybrid and copolymeric MP prepared by AAROP prove that their thermal characteristics and crystallinity can be opportunely manipulated using various filler types, which could be potentially useful in SLS applications.

Further information about the thermal resistance of the MP samples was obtained by TGA analysis. The traces are presented in their integral and differential forms in Figure 7. To enable comparison, the traces of PA6 MP are presented.

The visual inspection of the integral TGA traces in Figure 7a suggest that all PA12 homopolymer-based MP samples (curves 1–4) are significantly more resistant to pyrolysis than PA6 and show only one degradation step attributable to single degradation event. The copolymeric PA12-6 MP (curve 5) displays two degradation steps, the first one with onset above that of neat PA6 MP, and the second with onset below that in neat PA12 MP samples. This fact is in favor of the block-copolymeric structure of the PA12-6 MP. The derivative TGA curves shown in Figure 7b display single degradation events in all homopolymer PA12 MP samples with maximum degradation temperature T_D^{max} close to 470°C. The neat PA6 MP shows two close degradation events at 340–355°C. As expected, the PA12-6 copolymeric MP revealed two T_D^{max} values that correspond to the T_D^{max} of PA6 and of PA12. As the areas of the two peaks in Figure 7b curve 4 are

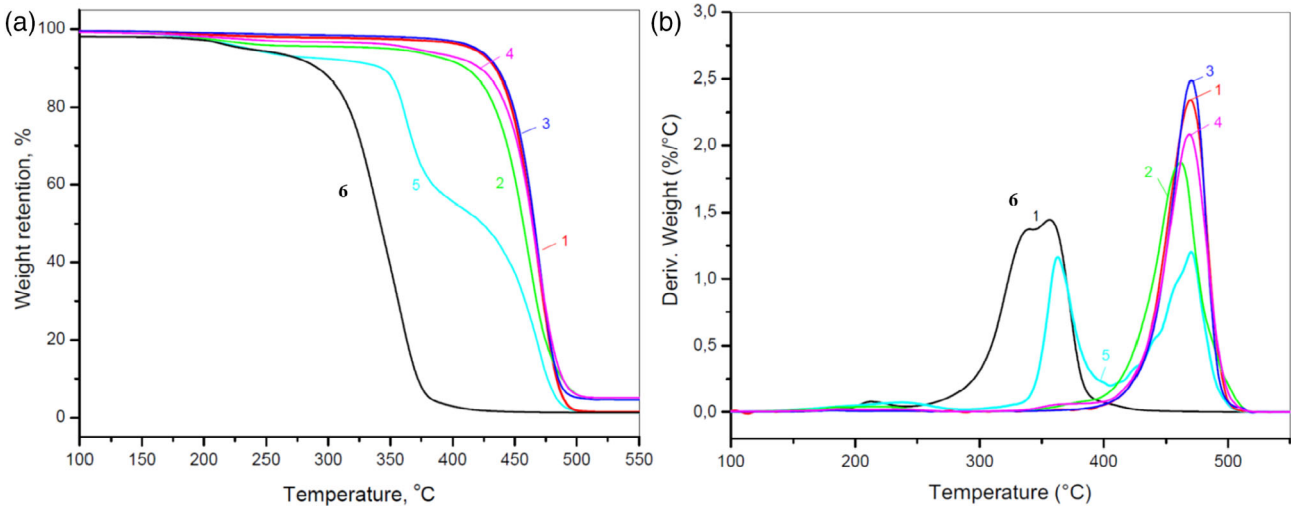

FIGURE 7 TGA traces of MP with different loads: a, Integral weight loss curves; b, First derivative curves. 1 – PA12; 2 – PA12-Fe; 3 – PA12-CB; 4 – PA12-Al; 5 – PA12-6; 6 – PA6 [Color figure can be viewed at wileyonlinelibrary.com]

TABLE 3 Thermal data extracted from the TGA traces of MP

Sample microparticles	Start degrad. Temp., T_D^{in} °C	Max. degrad. Temp. T_D^{max}, °C	Max. degrad. Rate, V_D^{max} %/°C	Carbon. residue at 550°C, %	Real load R_L, %
PA12	441.8	469.5	2.3	1.42	0.0
PA12-Fe	431.3	461.8	2.1	7.42	6.0
PA12-CB	441.6	470.3	2.5	4.59	3.2
PA12-Al	439.4	469.5	2.1	5.12	3.7
PA12-6	351.4 440.6	363.1 470.8	1.16 1.20	1.45	0.0

similar, the two comonomers are most probably presented in similar amounts in PA12-6 copolymer.

More data about the thermal degradation of PA12-based MP are presented in Table 3. The real filer content R_L was obtained on the basis of the carbonized residues at 550°C of the MP with and without filler according to Equation 1 (Table 2, last two columns). The payload in the hybrid MP varied between 3.2 and 6.0 wt%, which is higher than the amount of the respective load in the AAROP reaction mixture (2.0 wt%, in relation to the LL monomer). This fact, as already mentioned, can be explained with conversions of LL-to-PA12 significantly lower than 100%, wherein all the filler particles remain in the resulting polymer. Moreover, some chemical changes of the payloads above 500°C during the TGA carbonization leading to additional increase of this percentage cannot be excluded completely. As known from our previous studies on loaded polyamide MP, Fe concentrations of ca. 3%–5% wt. impart saturated magnetization values of about 12-14-emu/g.[21,23,24] The PA12-Al and PA12-Fe molded samples are expected to be electrical insulators due to the Maxwell-Wagner-Sillars polarization.[33] Meanwhile, the PA12-CB sample may be compression molded into plates with electrical conductivity up to 6–7 orders of magnitude higher than of the neat PA12 plates, similarly to what was observed with PA6-CB and CNT containing samples.[34] This induction of magnetic and electro-conductive properties could also be interesting for a potential use of hybrid PA12 MP in SLS.

The results in Table 3 indicate that the temperature of initial degradation (T_D^{in}) of neat PA12, PA12-CB and PA12-Al MP samples are close to 440°C. The second degradation event in the PA12-6 sample that is attributable to the PA12 fraction in it, starts at a similar temperature, and the pyrolysis of the PA6 fraction – at 351.4°C. As seen from curve 6 in Figure 7a, this is the T_D^{in} of the neat PA6 sample. Notably, the T_D^{in} of the PA12-Fe MP is with 10°C lower, suggesting some destabilization effect by the Fe filler. It can be explained with the much lower heat capacity of Fe (0.451 J/g.°C against 0.902 J/g.°C for Al) making it heat up faster than Al at equal other conditions and therefore concentrating more heat in its close vicinity, thus causing an earlier thermal degradation of PA12 matrix. For all PA12-based samples, the T_D^{max} values is with about 30°C higher than T_D^{in}, except for the PA6 fraction in the PA12-6 copolymer. The maximum degradation rate V_D^{max} is similar in all PA12 samples and reduces almost twice for the PA6 and PA12 segments in the PA12-6 copolymer.

3.5 | Structural studies by synchrotron WAXS and SAXS

It is generally accepted that the crystalline phase in polyamides is formed by hydrogen-bonded macromolecules arranged in layers. The two basic crystalline modifications designated the α and γ forms were established first in PA6[35,36] and later in PA12.[37] The main crystalline form of PA12 obtained by melt crystallization at atmospheric pressure is the γ form.[38] The α-PA12 is obtained under special conditions including precipitation from solution.[39] Our previous studies on the structure of hydrolytic PA12[40,41] showed that upon annealing above 140°C and/or orientation, the γ polymorph in oriented molded samples partially transforms into α-PA12 resulting in a higher α/γ ratio. The increase of the latter determines a growth in the elastic modulus and yield stress values, and causes reduction of the deformation at break. To the best of our knowledge, the crystalline structure of PA12 MP prepared by AAROP in solution, especially in the presence of metal- or carbon allotrope fillers, has never been studied before.

Figure 8 presents the synchrotron WAXS linear patterns of all PA12-based samples of this study, including also the as-prepared PA6 MP at 30°C (Figure 8a), the MP samples at 30°C after melting at 200°C (Figure 8b) and the patterns of a PA12-6 copolymeric sheet (Figure 8c) produced by compression molding of the respective PA12-6 MP. In the latter case in-beam heating in the 30–200°C range was applied.

The WAXS pattern of the neat PA12 MP (Figure 8a, curve 1) and of the two metal-containing samples

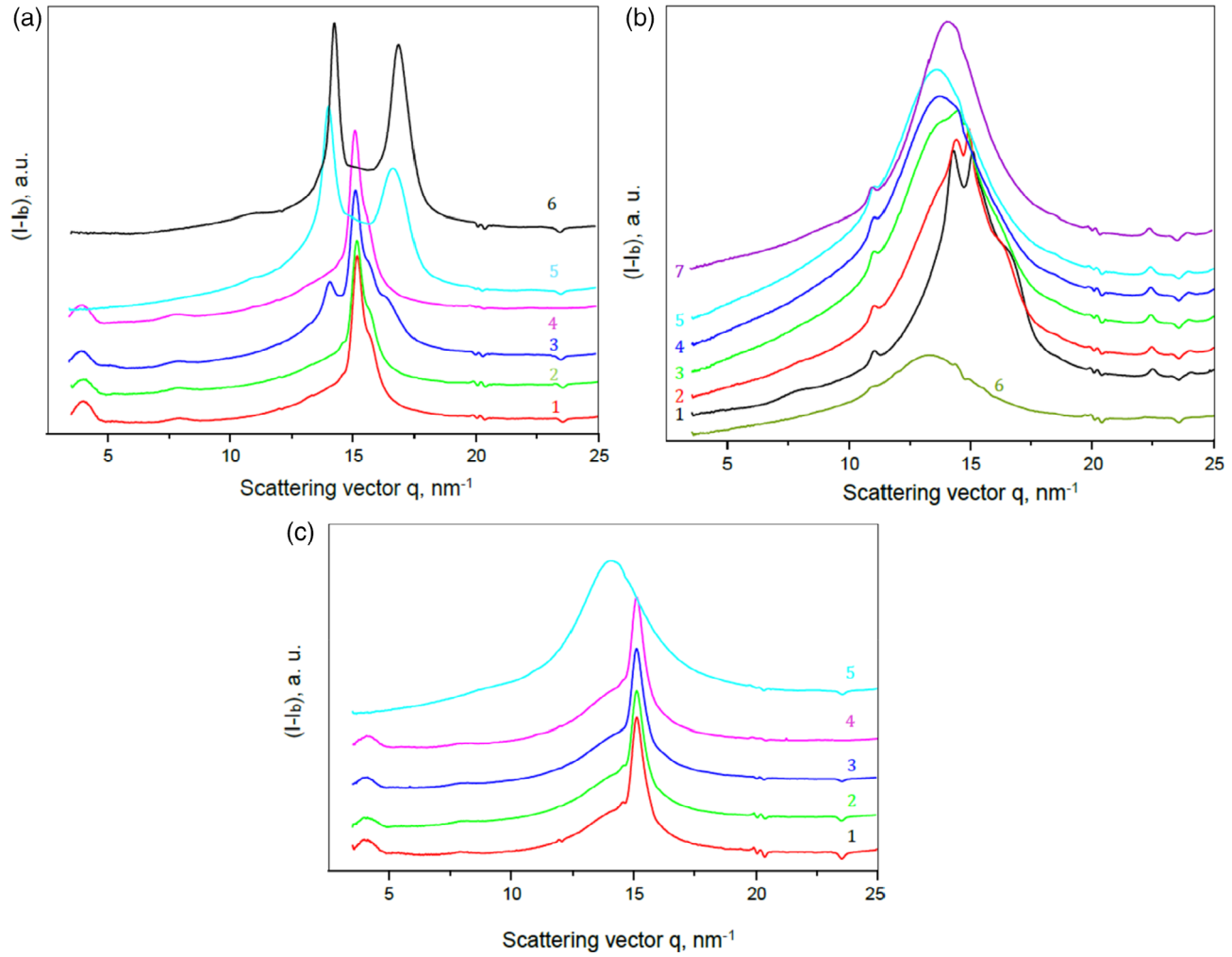

FIGURE 8 Linear synchrotron WAXS patterns of: a, PA12-based MP at 30°C; b, PA12-based MP samples after melting at 200°C, irradiated at 30°C; c, Copolymeric PA12-6 molded plate at different temperatures. For images a and b: 1– PA12; 2 – PA12-Fe; 3 – PA12-CB; 4 – PA12-Al; 5 – PA12-6; 6 – PA6. For image c: 1–30°C; 2–140°C; 3–160°C; 4–30°C after 160°C; 5–180°C; 6–200°C; 7–30°C after 200°C [Color figure can be viewed at wileyonlinelibrary.com]

PA12-Al and PA12-Fe (curves 2 and 4) reveal at 30°C a characteristic reflection centered at $q = 15.2$ nm^{-1} typical of a pseudo-hexagonal γ-PA12 phase. The PA12-CB MP sample (curve 3) shows two additional weaker reflections at $q = 14.2$ nm^{-1} and 16.4 nm^{-1} of some amounts of monoclinic α-PA12 polymorph whose presence could be related to specific nucleation during AAROP caused by the CB filler. This behavior was observed during the DSC recrystallization of this sample. In all patterns 1–4 weak reflections typical for the predominant γ-PA12 are also present with q values of ca. 4.0 and 8.0 nm^{-1}, attributable to $d\gamma_{020}$ and $d\gamma_{040}$, respectively (b-axis is the chain axis). Interestingly, in hydrolytic bulk PA12 these reflections are normally observed only in oriented samples.[40,41]

The copolymeric PA12-6 MP sample (Figure 8a, curve 5) contains mainly α-PA12 polymorph, with a WAXS pattern almost identical to the PA6 MP reference (curve 6) obtained by the same AAROP method. After melting the MP samples at 200°C and cooling to 30°C, that is, molding of the MP into films by in-beam heating, all PA12 homopolymers (curves 1–4 in Figure 8b) still contain mainly γ-polymorph. As expected based on the DSC study, melting of the PA12-6 copolymeric MP at 200°C leads to a completely amorphous, unable to crystalize structure. The WAXS analysis confirms the hypothesis that at 200°C, that is, in the melt and well above T_m of the higher-melting PA6 blocks found to be around 162°C (Table 2), transamidation reactions between PA12 and PA6 can occur. They should lead to the formation of statistical copolymers containing sequences of less than 4–5 repeat units of each type that would be unable to crystallize under cooling. In fact, if PA12-6 MP are compression molded in a hot press, transparent films with rubber-like elasticity are obtained. Annealing the latter at different

temperatures while irradiating in a WAXS synchrotron beamline (Figure 8c) shows that at 140, 160°C and at 30°C after heating at 160°C (curves 2–4), some residual crystallinity is still present in this sample, judging by the form of the main reflection at q = 14.5–15.0 nm. A completely amorphous halo characteristic of a totally disordered structure appears only after annealing for 5–7 min at 200°C and cooling down to 30°C (Figure 8c, curves 6, 7). Nevertheless, a narrow crystalline reflection at q = 11.0 nm^{-1} is still present in the latter, whose origin is not yet understood.

More data were extracted from the WAXS linear profiles in Figure 6 after their deconvolution by peak fitting performed as described earlier.[40,41] An example deconvolution of the PA12 MP sample is presented in Figure 9. All structural data extracted from the deconvoluted patterns at 30°C are displayed in Table 4. It shows that the X_c^{WAXS} values of all MP powders are in the range of 41%–46% dropping after melt recrystallization to 32%–33%, this decrease being independent on the filler type. Similar tendency was observed with the X_c^{DSC} values Table 2. In all neat and hybrid PA12 MP samples before and after recrystallization, the fraction of γ-PA12 predominates, the α/γ ratio being between 0.24–0.57. In the neat PA12 the melt recrystallization additionally decreases the α/γ value from 0.24 to 0.16. Notably, the X_c^{WAXS} and α/γ values of commercial hydrolytic and non-oriented PA12 were found to be 31.0% and 0.18, respectively,[41] that is, coinciding with the data of recrystallized neat PA12 MP in Table 4. The presence of metal fillers (Fe or Al) seem to promote the α-polymorph formation, especially after recrystallization of MP.

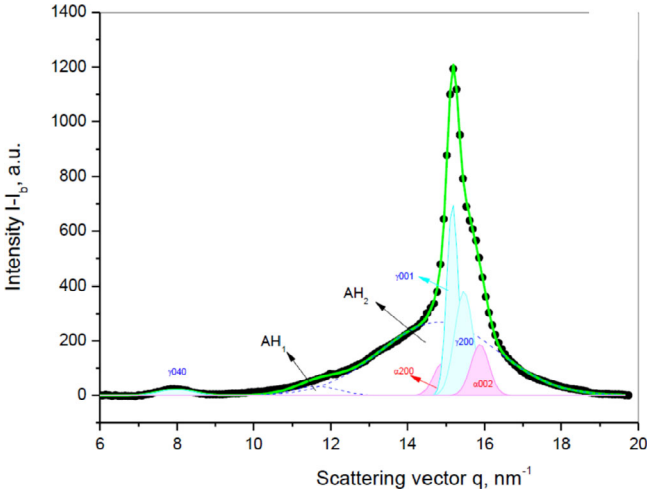

FIGURE 9 Example deconvolution of the PA12 MP sample. For more information, see refs. [39,40] [Color figure can be viewed at wileyonlinelibrary.com]

It is worth noting that the highest content of α-PA12 is observed in the PA12-CB (as prepared MP sample) decreasing slightly after its recrystallization. On the contrary, the α/γ ratio of the PA12-Fe and PA12-Al sample increases after recrystallization. Most probably the two metal payloads nucleate better the α-PA12 phase during its recrystallization.

In the as-prepared copolymeric PA12-6 MP sample a decisive difference is observed in the crystalline structure, as compared to the other MP samples, with a strong promotion of the α-phase formation, so that α/γ ≈ 12 (Table 4), which means that both PA12 and PA6 blocks form predominantly α-crystallites, confirmed also by the FTIR analysis (Figure 5). Our previous investigations on

TABLE 4 Structural data extracted from the WAXS patterns at 30°C

	Crystallinity index %				d-spacings, Å				
Sample designation	**α-Phase**	**γ-Phase**	X_c^{WAXS}	**α/γ**	α_{200}	α_{002}	γ_{001}	γ_{200}	γ_{040}
PA12	10.1	32.2	42.3	0.24	4.22	3.96	4.14	4.06	7.98
	4.5	**28.4**	**32.9**	**0.16**	**4.28**	**3.91**	**4.14**	**4.04**	**7.79**
PA12-Fe	10.7	35.3	46.0	0.30	4.24	3.95	4.14	4.03	7.86
	12.0	**19.6**	**31.6**	**0.61**	**4.25**	**4.09**	**4.16**	**4.12**	**7.74**
PA12-CB	14.7	25.9	40.6	0.57	4.43	3.83	4.14	4.00	7.89
	10.5	**23.4**	**33.9**	**0.45**	**4.37**	**4.06**	**4.15**	**4.08**	**7.69**
PA12-Al	13.7	28.5	42.2	0.48	4.21	4.00	4.14	4.03	7.93
	11.9	**21.6**	**33.5**	**0.55**	**4.35**	**4.08**	**4.15**	**4.12**	**7.56**
PA12-6	16.3*	1.7	31.8	11.9	4.48	3.69	4.07	—	—
	13.0**	0.8			4.46	3.79	4.37		
	0.0	**0.0**	**0.0**	—	—	—	—	—	—

Note: For each sample, the values of the respective MP are typed with normal font, the bolded numbers are obtained after melting of the MP, at 30°. *Values corresponding to the PA12 fraction in the copolymer; ** Values corresponding to the PA6 fraction of the copolymer.

the structure of PA6 MP[22] showed that during AAROP in solution PA6 crystallizes mostly in its α-crystalline form. The high α/γ ratio in PA12-6 sample can be explained with the presence of crystallizable PA6 blocks serving as α-phase nucleants. Heating above 200°C and cooling down to 30°C results in almost completely disordered copolymer (Figure 8b curve 5, Figure 8c curve 7). Apparently, copolymerization during the AAROP along with the introduction of various payloads into the resulting copolymeric MP could be a tool for changing the crystalline structure and therefore the melting behavior of the pulverulent materials so produced.

Table 4 shows also minor oscillations of the d-spacings values of all PA12 MP samples before and after recrystallization. These values almost coincide with those of commercial non-oriented PA12 granules[40] meaning that after melting both kind of samples are of identical crystalline structure.

Additional information about the semicrystalline PA12-based samples of this study was obtained with synchrotron SAXS of the PA12 MP powders: as synthesized, after melt recrystallization, as well as of compression molded PA12-6 MP, irradiated at different temperatures. The SAXS curves of all samples are presented in Figure 10.

The Lorentz-corrected linear SAXS patterns of all PA12-based MP samples and the PA6 MP control obtained at 30°C are presented in Figure 10a. Well-expressed lamellar structure characterized by a strong SAXS peak at $q = 0.764\ \mathrm{nm}^{-1}$ was found only in the copolymeric PA12-6 MP, with a Bragg long spacing $L_B = 82$ Å. The rest of the MP samples did not display resolved SAXS peaks. Such phenomenon was observed and studied previously with PA6 MP.[19] There, the absence of a Bragg peak was explained with the extensive micron-sized porosity of the polyamide MP that makes

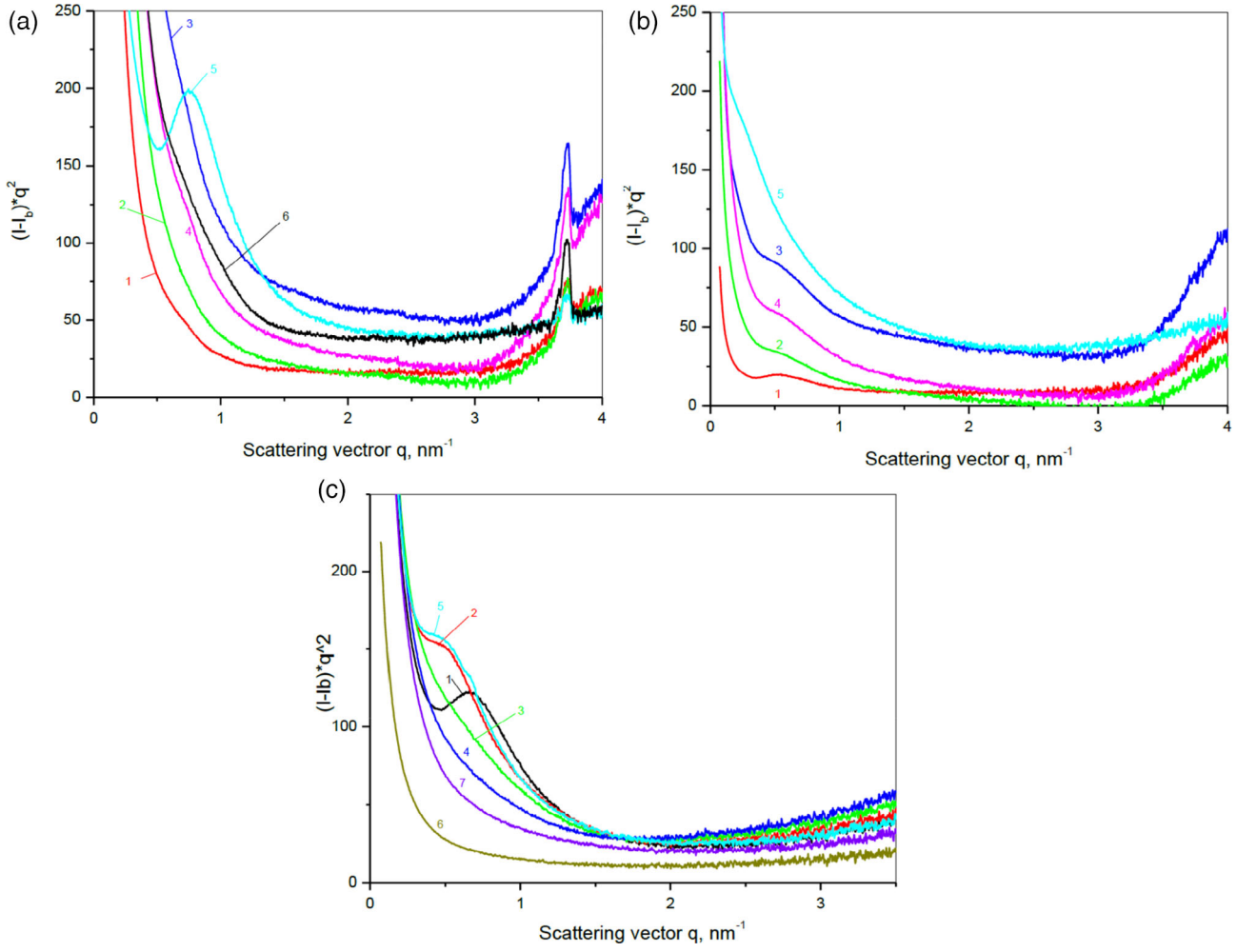

FIGURE 10 Linear synchrotron SAXS patterns of: a, PA12-based MP at 30°C; b, PA12-based MP samples after melting at 200°C, irradiated at 30°C; c, Copolymeric PA12-6 molded plate at different temperatures. For images a and b: 1– PA12; 2 – PA12-Fe; 3 – PA12-CB; 4 – PA12-Al; 5 – PA12-6; 6 – PA6. For image c: 1–30°C; 2–100°C; 3–140°C; 4–160°C; 5–30 after 160°C; 6–250°C; 7–30°C after 250°C [Color figure can be viewed at wileyonlinelibrary.com]

negligible the density gradient between the crystalline and amorphous phases.

This is the most probable explanation also with the PA12-based samples of this study. All MP samples in Figure 10a show also a narrow SAXS peak at $q = 3.72\ \text{nm}^{-1}$ corresponding to 16.8 Å and attributable to the nanoporosity of the polyamide MP.[20]

Figure 10b displays the linear SAXS patterns of all microparticulate samples after their melting at 200°C and recrystallization at 30°C. All homopolymer samples display a weak and poorly resolved L_B with values around 100 Å and no peaks for nanoporosity around 3.7 nm^{-1}. It can be therefore hypothesized that upon melting and recrystallization in the films, the phase contrast between the amorphous and crystalline PA12 improves due to the disappearance of the porosity. Only the PA12-6 sample in Figure 10b does not possess lamellar morphology due to its total amorphization upon melting already proved by DSC and WAXS.

As seen from Figure 10c, the complete amorphization of the PA12-6 compression molded film obtained from the respective MP is not instant and, up to a certain temperature, could be inversed. Thus, the initial molded film at 30°C (curve 1) has a L_B of 95 Å. Increasing the temperature to 100°C (curve 2) still maintains the SAXS peak, while after 5 min at 140 and 160°C (curves 3, 4) the lamellar organization disappears. After such temperatures the lamellar stack morphology can still be recovered since upon cooling to 30°C the SAXS peak reappears (curve 5). However, heating at 200–250°C for 3 min or longer (curve 6) leads to an irreversible amorphization of the copolymeric PA12-6 sample and the final sample at 30°C (curve 7) produces no Bragg peak. Apparently, complete melting of the PA12-6 sample and elevated temperatures are necessary for the transamidation reaction to take place that will produce a statistical copolymer with PA12 and PA6 blocks below a certain critical length impossible to form ordered domains.

3.6 | Mechanical properties in tension

To perform this study, all PA12-based MP samples, as well as neat PA6 and PA12 MP were compression-molded in a hot press producing 1 mm thick films. Standard tests samples were cut from these films and studied in tension to obtain the respective stress–strain curves presented in Figure 11. The tests were performed with 8–10 standard specimens of each sample conditioned at 65% relative humidity for 30 days. The results extracted from the curves are presented in Table 5.

Figure 11 shows that the neat PA6 and PA12 (curves 1 and 2), as well as PA12-Fe and PA12-CB (curves 3, 4),

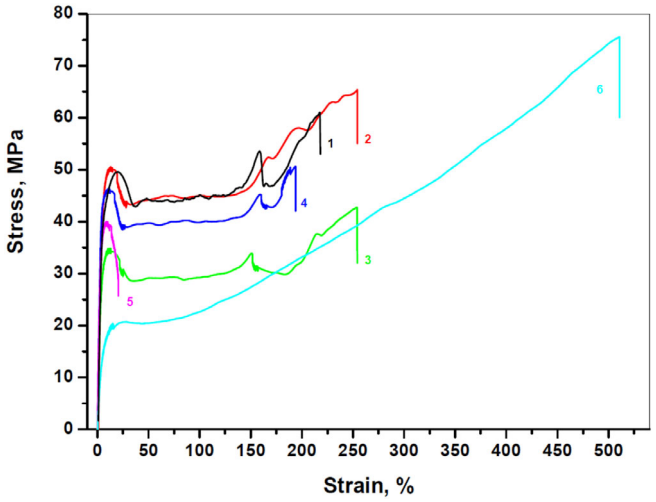

FIGURE 11 Representative stress–strain curves of PA12-based films compression-molded from microparticles. 1 – PA6; 2 – PA12; 3 – PA12-Fe; 4 – PA12-CB; 5 – PA12-Al; 6 – PA12-6 [Color figure can be viewed at wileyonlinelibrary.com]

all of them obtained from MP, display the typical mechanical behavior of non-oriented polyamides. The stress–strain curves have well-expressed yield points at deformation levels $\varepsilon \approx 10\%$ and close values of the stress at yield σ_y and stress at break σ_{br} (i.e., only weak strain hardening is observed), best expressed in the neat PA12 and PA6. These four samples show also a typical plastic flow plateau in the deformational range of 50%–250%. Apparently, the distributions of the Fe and CB fillers is very good since their σ_{br} values are close to that of the neat PA12. This is not the case with the Al particles that cause brittle failure of the PA12-Al composite sample right after its yield point. The reason for this could be the different sizes of these fillers: about 30 μm for Al, 3–5 μm for Fe, while for the PA12-CB film nanoscale dispersed system is expected.

As regards the E modulus values, in the PA12, PA12-Fe and PA12-Al they are all around 1.3 GPa. The PA12-CB sample in Table 5 shows a statistically higher values, most probably due to the nanoscale dispersion of the filler. The highest E-modulus of 1.59 GPa was shown by the neat PA6 sample.

As seen from Table 5, the mechanical data of the compression molded films produced from MP synthesized by AAROP favorably compare to those of commercial hydrolytic PA12 (HPA12). All of them display an increase of E with 35–55%, meanwhile the σ_y and especially the σ_{br} values remain considerably higher than those of HPA12. All these data confirm once again that the method used in this study resulted in the production of neat and hybrid PA12 MP with high enough molecular weight ensuring rather good mechanical properties of the respective composite materials.

TABLE 5 Mechanical data extracted from the stress–strain curves in Figure 11

Sample designation	Elastic modulus E (GPa)	Stress at yield σ_y, (MPa)	Stress at break σ_{br}, (MPa)	Elongation at break ε_{br}, (%)
PA6	1.59 ± 0.05	50.6 ± 3.0	58.6 ± 4.0	218 ± 10
PA12	1.30 ± 0.05	51.2 ± 2.2	63.7 ± 3.4	301 ± 37
PA12-Fe	1.32 ± 0.08	36.6 ± 1.7	40.6 ± 1.4	240 ± 12
PA12-CB	1.49 ± 0.03	43.7 ± 3.1	44.7 ± 3.6	172 ± 42
PA12-Al	1.31 ± 0.06	37.3 ± 2.0	—	8.7 ± 0.2
PA12-6	0.38 ± 0.05	21.3 ± 2.0	68.8 ± 5.3	499 ± 21
HPA12[a]	0.96 ± 0.07	32.3 ± 3.0	36.1 ± 5.6	188 ± 11

[a]Commercial hydrolytic PA12 (Grilamid L25 H) of EMS Grivory.

The stress–strain curves of the copolymeric PA12-6 sample (Figure 11, curve 6) is characterized by low E modulus, low σ_y but with superior σ_{br} being higher than that of the neat PA12. The PA12-6 film is extremely ductile with ε_{br} values close to 500% and strong strain hardening. A possible reason for this unusual tensile behavior of the PA12-6 sample could be the plasticizing effect of lower molecular weight oligomers formed during the compression molding of this specific MP sample due to partial thermal degradation of the latter. In favor of such a hypothesis is the weight loss of up to 3 wt% found in the PA12-6 MP during the TGA test at 210–215°C (Figure 7, curve 5). However, the neat PA6 MP that produces the same weight loss at this temperature (Figure 7, curve 6) displays a strass-strain curve after compression molding (Figure 11, curve 1) being analogous to that of PA12 wherein no degradation around 210°C was found. Moreover, the E-value of 1.59 GPa of the PA6 sample (Table 5) was the highest of all samples tested which excludes any possible plasticization effects in this sample and, consequently, in the PA12-6 sample. Therefore, the peculiar tensile behavior of the PA12-6 compression molded MP cannot be related to plasticizing effects caused by partial thermal degradation. A much more probable cause is the specific crystalline structure of this sample (Figure 8c, curve 1) that is intermediate between those of PA12 and PA6.

4 | CONCLUSIONS

The work presented in this paper introduces the following innovations in the area of the production of PA12 powders. First, neat, hybrid and copolymeric PA12 MP are produced by a one-pot chemical reaction in-situ, at temperatures substantially lower than those used in the commercial hydrolytic process, at a pressure of 1 atm. Second, the semicrystalline PA12 MP form very rapidly and encapsulate the filler particles existing in the reaction mixture, thus producing hybrid MP that are easily separated from the reaction mixture. This synthetic method is very versatile because it allows the microencapsulation of quite distinct fillers such as metal micro- or nanoparticles, carbon allotropes and permits also the synthesis of copolymeric powders. The hybrid MP represent spheroid porous structures with sizes in the 20–100 μm range, in which the semicrystalline polyamide covers (entraps) several metal or many CB particles. In the latter case, the CB particles can also appear on the surface of the spheroid MP. Third, the resulting loaded MP can be further melt-processed to hybrid or laminate composites, or, alternatively, used in their as-prepared powder-like form for additive manufacturing purposes. The latter should be possible, since the PA12 neat and hybrid MP of this study possess a thermal behavior very close to that of the commercial PA12, due to an almost identical crystalline structure. Compression molded films produced from the MP display mechanical properties in tension superior to that of commercial hydrolytic PA12. The possibility to produce PA12-6 copolymeric MP could also be interesting for applications in additive production techniques, since the initially highly crystalline powders could be transformed by SLS into transparent final articles - with lower crystallinity or completely amorphous, depending on the SLS processing parameters. Finally, it is expected that the application of these hybrid PA12 powder in additive manufacturing will lead to the production of 3D articles not only with good mechanical particles but also possessing controllable magnetic properties and/or electroconductivity.

ACKNOWLEDGMENTS

The authors gratefully acknowledge the financial support of *Fundação para a Ciência e Tecnologia* (FCT), project UID/CTM/50025/2019. Special thank is due to the ALBA synchrotron governance for financing our WAXS/SAXS experiments at NCD SWEET beamline in the framework of the project ID 2018/022726.

N. Dencheva is also grateful for the financial support of FCT in the frames of the personal program contract CTTI-51/18-IPC. J. Braz acknowledges the support of the FCT UI/BD/150854/2021 PhD grant.

CONFLICT OF INTEREST

The authors declare no potential conflict of interest.

ORCID

Nadya Vasileva Dencheva https://orcid.org/0000-0003-1698-553X
Joana Filipa Barros Braz https://orcid.org/0000-0002-6342-1967
Zlatan Zlatev Denchev https://orcid.org/0000-0002-9057-9380

REFERENCES

[1] H. Ulf, W. Rohde-Liebenau, in *Polymer Data Handbook* (Ed: J. E. Mark), Oxford University Press, New York **1999**, p. 225.
[2] G. Wypych, *Handbook of Polymers*, ChemTec Publishing, Toronto **2016**, p. 246.
[3] A. Borić, A. Kalendová, M. Urbanek, T. Pepelnjak, *Polymer* **2019**, *11*, 1248.
[4] K. Jovic, K. Unold, S. Naumann, M. Ullrich, F. G. Schmidt, M. R. Buchmeiser, *Macromol. Mat. Eng.* **2016**, *301*, 423.
[5] M. Mohammadi, S. Ahmadi, I. Ghasemi, M. Rahnama, *Polym. Eng. Sci.* **2019**, *59*, 1529.
[6] T. Novitsky, L. J. Mathias, *J. Polym. Sci. Part A: Polym. Chem.* **2011**, *49*, 2271.
[7] DIN EN ISO/ASTM 52900: Additive manufacturing - General principles and terminology, **2015**.
[8] J. Schmidt, M. Sachs, S. Fanselow, M. Zhao, S. Romeis, D. Drummer, K.-E. Wirth, W. Peukert, *Chem. Eng. Sci.* **2016**, *156*, 1.
[9] J. Schmidt, M. Sachs, C. Blümel, B. Winzer, F. Toni, K.-E. Wirth, W. Peukert, *Powder Technol.* **2014**, *261*, 78.
[10] R. D. Goodridge, C. J. Tuck, R. J. M. Hague, *Prog. Mater. Sci.* **2012**, *57*, 2229.
[11] G. Wang, P. Wang, Z. Zhen, W. Zhang, J. Ji, *Mater. Des.* **2015**, *87*, 656.
[12] K. Shahzad, J. Deckers, S. Boury, B. Neirinck, J.-P. Kruth, J. Vleugels, *Ceram. Int.* **2012**, *38*, 1241.
[13] D. Drummer, M. Medina-Hernández, M. Drexler, K. Wudy, *Procedia Engineering* **2015**, *102*, 1918.
[14] H. Chung, S. Das, *Mat. Sci. Eng. A* **2006**, *437*, 226.
[15] M. Krantz, Z. Hui, J. Zhu, *Powder Technol.* **2009**, *194*, 239.
[16] Y. Zhou, S. Xi, Y. Huang, M. Kong, Q. Yang, G. Li, *Mater. Des.* **2020**, *190*, 108578.
[17] H. Senff, C. Gaborian (Arkema), US 0113661A1, **2010**.
[18] Z. Denchev, N. Dencheva (University of Minho), PT10767914A, **2014**.
[19] C. Cano-Raya, N. Dencheva, J. F. Braz, M. Malfois, Z. Denchev, *J. Appl. Polym. Sci.* **2020**, *137*, 49131.
[20] N. Dencheva, S. C. Oliveira, J. Braz, D. Getya, M. Malfois, Z. Denchev, I. Gitsov, *Catalysts* **2021**, *11*, 239.
[21] N. Dencheva, Z. Denchev, S. Lanceros-Méndez, T. A. Ezquerra, *Macromol. Mat. Eng.* **2016**, *301*, 119.
[22] N. Dencheva, D. Vale, Z. Denchev, *Polym. Eng. Sci.* **2017**, *57*, 806.
[23] N. Dencheva, J. Braz, D. Scheibel, M. Malfois, Z. Denchev, I. Gitsov, *Catalysts* **2020**, *10*, 767.
[24] N. Dencheva, F. D. Oliveira, J. F. Braz, Z. Denchev, *Eur. Polym. J.* **2020**, *122*, 109375.
[25] J. B. González, N. González, C. Colldelram, L. Ribó, A. Fontserè, G. J. Mañas, J. Villanueva, M. Llonch, G. Peña, A. Gevorgyan, Y. Nikitin, J. C. Martínez, C. Kamma-Lorger, E. Solano, I. Sics, S. Ferrer, M. Malfois, *NCD-SWEET beamline upgrade, presented at MEDSI2018*, France, Paris **2018**.
[26] G. Ashiotis, A. Deschildre, Z. Nawaz, J. P. Wright, D. Karkoulis, F. E. Picca, J. Kieffer, *J. Appl. Crystallogr.* **2015**, *48*, 510.
[27] J. Šebenda, J. Macromol, *Sci. Part A - Chem.* **1972**, *6*, 1145.
[28] L. Ricco, O. Monticelli, S. Russo, A. Paglianti, A. Mariani, *Macromol. Chem. Phys.* **2002**, *203*, 1436.
[29] F. Dan, C. Vasiliu-Oprea, *J. Appl. Polym. Sci.* **1996**, *62*, 1517.
[30] A. Almansoori, R. Masters, K. Abrams, J. Schäfer, T. Gerling, C. Majewski, C. Rodenburg, *Plasma Processes Polym.* **2018**, *15*, e1800032.
[31] M. Porubská, O. Szöllős, A. Kóňová, I. Janigová, M. Jašková, K. Jomová, I. Chodák, *Polym. Degrad. Stab.* **2021**, *97*, 523e531.
[32] S. Gogolewski, K. Czerntawska, M. Gastorek, *Colloid Polym. Sci.* **1980**, *258*, 1130.
[33] C. Breda, N. Dencheva, S. Lanceros-Méndez, Z. Denchev, *J. Mat. Sci.* **2016**, *51*, 10534.
[34] F. Oliveira, N. Dencheva, P. Martins, S. Lanceros-Méndez, Z. Denchev, *eXPRESS Polym. Lett.* **2016**, *10*, 160.
[35] D. R. Holmes, C. W. Bunn, D. J. Smith, *J. Polym. Sci.* **1955**, *17*, 159.
[36] H. Arimoto, M. Ishibashi, M. Hirai, Y. Chatani, *J. Polym. Sci. Part A General Papers Article* **1965**, *3*, 317.
[37] M. I. Kohan, *Nylon plastics*, John Wiley & Sons, NY, USA **1973**.
[38] M. H. J. Koch, W. H. de Jeu, *Macromolecules* **2003**, *36*, 1626.
[39] T. Ishikawa, S. Nagai, N. Kasai, *J. Polym. Sci., Polym. Phys. Ed.* **1980**, *18*, 291.
[40] N. Dencheva, T. Nunes, M. J. Oliveira, Z. Denchev, *J. Polym. Sci. Part B: Polym. Phys. Ed.* **2005**, *43*, 3720.
[41] N. Dencheva, Z. Denchev, M. J. Oliveira, T. G. Nunes, S. S. Funari, *J. Appl. Polym. Sci.* **2008**, *109*, 288.

How to cite this article: N. Vasileva Dencheva, J. F. B. Braz, Z. Z. Denchev, *J. Appl. Polym. Sci.* **2022**, *139*(11), e51784. https://doi.org/10.1002/app.51784